6-10-2019

The cation exchange behavior of tylosin in loess-derived soil

Jaime J. Call
University of Tennessee, Knoxville

Michael E. Essington
University of Tennessee, Knoxville

Sudipta Rakshit
Tennessee State University

Recommended Citation

J.J. Call, M.E. Essington, S. Rakshit, "The cation exchange behavior of tylosin in loess-derived soil", Chemosphere, Volume 233, 2019, Pages 615-624, ISSN 0045-6535, https://doi.org/10.1016/j.chemosphere.2019.06.028.

The Cation Exchange Behavior of Tylosin in Loess-Derived Soil

Jaime J. Call and Michael E. Essington*
Department of Biosystems Engineering & Soil Science
2506 E.J. Chapman Dr.
The University of Tennessee
Knoxville, TN 37996
USA

Sudipta Rakshit
Department of Agricultural & Environmental Sciences
3500 John A. Merritt Blvd.
Tennessee State University
Nashville, TN 37209
USA

*Corresponding author (messington@utk.edu)
Telephone: 865-974-7266
Fax: 865-974-4514

Declarations of interest: none

ABSTRACT

Tylosin (Tyl) is a veterinary antibiotic commonly used in swine and poultry production. Due to metabolic inefficiencies, it enters the environment through manure applications. Ion exchange is an important retention mechanism for Tyl, particularly for smectite clay. The objectives of this study are to characterize the exchange interactions of Tyl with common soil cations in subsoil horizons that contain smectite and to investigate the interactions using in situ Fourier transform infrared (FTIR) spectroscopy. Adsorbed Tyl in pH neutral, smectitic subsoil horizons is divided into exchangeable and nonexchangeable forms. The percentage of adsorbed Tyl that is exchangeable varies from 36% to 43% when Na^+ is the competing cation, and from 57% to 66% when Ca^{2+} competes. In NaX-TylX binary exchange systems, neither Na^+ nor Tyl^+ is preferred by the clay exchange phase, and the Vanselow selectivity coefficients (K_V) for the NaX→TylX exchange reaction range between 0.79 and 1.41. In the CaX_2-TylX systems, Tyl^+ is preferred by the clay exchange phase when the equivalent fraction of TylX (E_{TylX}) is less than 0.4. The K_V values for the CaX_2→TylX exchange reaction are at a maximum at the lowest E_{TylX} values, with $17.6 < K_V < 58.1$, then decrease with increasing E_{TylX} to $1.34 < K_V < 6.28$. Adsorbed Tyl masks the *CEC* of the soil clays; the effect is greatest in systems that are initially Tyl-saturated, and is attributed to the steric effects of the large Tyl molecule. In situ FTIR indicates that Tyl interacts with soil iron oxides through the dimethylamine moiety.

Keywords: Antibiotic, exchange selectivity, Vanselow, x-ray diffraction, ATR-FTIR

Abbreviations: ATR-FTIR, attenuated total reflectance Fourier transform infrared spectroscopy; *CEC*, cation exchange capacity; DDI, distilled-deionized water; HATR, horizontal attenuated total reflectance; HPLC, high pressure liquid chromatography, Tyl, tylosin; VM, Visual MINTEQ

1. Introduction

Tylosin (Tyl) is a broad-spectrum macrolide antibiotic first isolated from a strain of *Streptomycetes fradiae* in soil from Thailand (Hamill et al., 1961). The antibiotic is commonly used in swine and poultry production as a prophylactic and for the treatment of microbial infections. It is also used as a dietary supplement to improve feed efficiency and to enhance growth (Kumar et al., 2005). Veterinary-grade Tyl is sold as either a tartrate or phosphate salt (Tylan®, Elanco, Greenfield, IN), which also contains minor amounts of other antimicrobial agents, including desmycosin, macrocin, relomycin, and desmycinosyl tylosin (Fish and Carr, 1986). Tylosin consists of a 16-membered lactone ring with linked mycaminose and mycarose sugars radiating from ring position 5, and the sugar mycinose attached at position 14 (Fig. 1). The compound is relatively hydrophilic, with a water solubility of approximately 5.5 mmol L^{-1} and an octanol-water partition coefficient (log K_{ow}) of 1.15 to 2.50 (McFarland et al., 1997; Wollenberger et al., 2000; Loke et al., 2002). The dimethylamine functional group is protonated in neutral to acidic solutions ($pK_a = 7.50 \pm 0.13$) (Qiang and Adams, 2004).

Animal manure application to agricultural lands is the primary mode of Tyl entry into the environment (Joy et al., 2013; Soni et al., 2015; Luby et al., 2016; Sura et al., 2016; Dungan et al., 2017). An important retention mechanism of Tyl by soil and soil minerals is cation exchange, which occurs through the protonated dimethylamine functional group. Several studies have illustrated a correlation between soil clay content and adsorption intensity and capacity, as well as the influence of background electrolyte type and concentration on Tyl adsorption. Rabølle and Spliid (2000) studied Tyl adsorption by soils that varied in clay content, cation exchange capacity (*CEC*), and organic C and observed adsorption intensity to increase with increasing clay content. They also noted that Tyl adsorption was not correlated to soil *CEC* or organic C. Similar

findings have been reported by others (Chander et al., 2005; Allaire et al., 2006; ter Laak et al., 2006). In addition, ter Laak et al. (2006) observed Tyl retention by clay loam and loamy sand soil to decrease with increasing pH and with increasing ionic strength. Sassman et al. (2007) noted that Tyl adsorption intensity was strongly correlated to clay content, *CEC*, and surface area, but only weakly correlated to organic C content. They also observed the retention of Tyl to be greater in smectite dominated soils relative to those dominated by kaolinite, and that NH_4 acetate could provide the nearly complete removal of adsorbed Tyl when added to a methanol extractant. In addition, Lee et al. (2014), Srinivasan et al. (2014), and Stromer et al. (2018) have all illustrated the strong correlation of Tyl adsorption to the soil properties and experimental conditions that influence ion exchange: greater retention in smectite dominated soils relative to soils dominated by metal oxides and kaolinite; increased retention with decreasing pH and ionic strength; and greater adsorption when the ionic strength is controlled by monovalent (e.g., $NaNO_3$) relative to divalent salts (e.g., $Ca(NO_3)_2$).

Bewick (1979) observed higher Tyl adsorption by Na- and Ca-saturated montmorillonites relative to illite and kaolinite, and attributed this finding to the expansiveness of the montmorillonites. It was also shown that the displacement of Tyl from the exchange complex by Ca^{2+} was more difficult than the displacement of Na^{+}. Essington et al. (2010) and Zhang et al. (2013) examined the adsorption of Tyl by montmorillonite and kaolinite as a function pH, ionic strength, and the dominant electrolyte cation. Tylosin adsorption was greater in montmorillonite relative to kaolinite systems, decreased with increasing pH and ionic strength, and was greater in $NaNO_3$ systems relative to $Ca(NO_3)_2$ systems. Further, Tyl retention as a function of pH could be modeled by considering only outer sphere surface complexation. Zhang et al. (2013) also illustrated the intercalation of Tyl into montmorillonite using x-ray diffraction.

The hypothesis that ion exchange is an important retention mechanism for Tyl in soil was directly tested by Call et al. (2019). They examined the exchange selectivity of Tyl relative to Ca^{2+} and with Na^{+} in reference vermiculite and montmorillonite systems using binary exchange isotherms. They found Tyl to intercalate montmorillonite, but not vermiculite, and that >41% of the Tyl adsorbed by montmorillonite was exchangeable in systems dominated by Na^{+}, decreasing to >12% in systems dominated by Ca^{2+}. The exchange isotherms also demonstrated that Tyl was preferred by the smectite exchange phase relative to both Na^{+} and Ca^{2+}. The importance of cation exchange as a retention mechanism for Tyl was confirmed using infrared spectroscopy. It was also shown that polar and covalent surface interactions through carbonyl functional groups were responsible for the nonexchangeable forms of adsorbed Tyl.

In this study, the selectivity of adsorbed Tyl relative to common soil cations addressed by Call et al. (2019) for reference smectite is investigated in soil systems that contain smectite clay. The principal objective of the research was to determine if the preference of Tyl for the exchange phase relative to both Na^{+} and Ca^{2+} is also present in soil smectite. Binary exchange isotherms were developed to characterize Tyl exchange with Na^{+} and Ca^{2+}, to establish exchange preference, and to determine the distribution between exchangeable and nonexchangeable forms of the adsorbed Tyl. Adsorbed Tyl was characterized using in situ ATR-FTIR spectroscopy to evaluate retention mechanisms. The IR spectra of Tyl adsorbed on hematite was also examined; the hematite was used as a surrogate for soil iron oxides.

2. Materials and methods

2.1 Chemicals

Veterinary-grade Tyl tartrate was obtained from Elanco (Greenfield, IN) for use in the exchange studies and consists of 95.5% Tyl, 3.1% desmycosin, and 1.4% macrocin. Analytical

grade Tyl tartrate (98.8% Tyl) was obtained from Sigma-Aldrich and used as a standard for the chemical analysis of the equilibrium exchange systems. Other chemicals used include distilled-deionized (DDI) water (carbon dioxide free, >18 Ω; Barnstead E-pure system) and analytical or HPLC grade compounds (Fisher Scientific, Fair Lawn, NJ). Hematite was prepared using the method described by Rakshit et al. (2017) and Sallman et al. (2018). Briefly, a 500-mL volume of 2 M $FeCl_3$ was slowly added to a 500-mL volume of 5.4 M NaOH while continuously stirred. The resulting precipitate was aged in a sealed Pyrex glass bottle for 8 days at 101°C. The precipitate was centrifuge-washed with DDI until an electrical conductivity of the supernatant liquid was <5 μS cm^{-1}. X-ray diffraction was used to confirm the precipitate was hematite without detectable impurities. The suspension was freeze-dried, and the hematite stored dry at room temperature.

2.2 Soils

Soil samples were collected from the University of Tennessee Milan Research and Education Center in Milan, TN (35° 56′ N, 88° 43′ W, 125 m elevation). The samples were obtained from the 15-30 cm and 30-46 cm depth increments of a Loring silt loam soil (Oxyaquic Fragiudalfs) which represent the Bt1 and Bt2 horizons and contain approximately 23% to 27% clay (Lindbo et al., 1994) and < 1 g kg^{-1} organic carbon (Jagadamma et al., 2019). The clay mineralogy of the soil samples was determined through x-ray diffraction (described below). The soil samples were air dried, disaggregated, passed through a 2 mm sieve, and then Na-saturated by repeated centrifuge washings with 1 M NaCl. The <2 μm size separate was isolated using Stoke's Law sedimentation with Na-saturated soil. The clay fraction was repeatedly centrifuge washed with DDI water to remove entrained salt, then freeze-dried. Clay subsamples were also Ca- or Tyl-saturated with repeated centrifuge washes of Na-saturated samples with either 1.0 M

137 $CaCl_2$, or 0.004 M or 0.01 M Tyl tartrate. Following the removal of entrained salts with DDI
138 water, the samples were freeze dried.

139 The cation exchange capacity (*CEC*) of the Bt1 and Bt2 clay separates was determined on
140 replicate samples using pH 7.2 Ca-acetate saturation, followed by NH_4-acetate displacement
141 (modified from Jackson, 2005). The clay samples were centrifuge washed 3 times with pH 7.2
142 1.0 M Ca-acetate to remove native exchangeable cations and to saturate the exchange complex
143 with Ca. Entrained Ca-acetate was then removed by centrifuge washing 3 times with DDI.
144 Finally, the Ca-saturated samples were centrifuge washed 3 times with pH 7.2 1 M NH_4-acetate,
145 the supernatant liquid collected into a 100 mL volumetric flask, brought to volume with NH_4-
146 acetate, and filtered through qualitative-grade filter paper. The NH_4-acetate extracts were stored
147 under refrigeration until analyzed for Ca. The Ca concentration in the extract is a direct measure
148 of the *CEC*. The mean *CEC* (± sd) of the Bt1 clay separate was 43.9 ± 1.9 $cmol_c\ kg^{-1}$, and that of
149 the Bt2 separate was 36.1 ± 1.9 $cmol_c\ kg^{-1}$.

150 *2.3 Binary exchange isotherms*

151 Binary exchange isotherms were developed using 0.5 g of the Bt1 and Bt2 clay separates
152 in 50 mL polyethylene centrifuge tubes. The centrifuge tubes were wrapped in aluminum foil to
153 minimize Tyl photolysis. The exchange experiments were performed in triplicate and initiated
154 with clay samples that were initially Tyl- or Na-saturated for Tyl-Na exchange, or Tyl- or Ca-
155 saturated for Tyl-Ca exchange. The soil clays were introduced to a 30 mL volume of solution
156 containing varied ratios of Tyl to Na, or Tyl to Ca, such that the total normality was 0.004 N.
157 Centrifuge tubes without solids were used as controls for each exchange experiment. These
158 control blanks were duplicated for each cation ratio in the experiment and used to determine Tyl
159 mass balance, total Cl and tartrate concentrations for ion speciation modeling, and to compute

total adsorbed concentration of Tyl. The suspensions and the blanks were equilibrated for 18 hours on an orbital shaker at ambient temperature (20-22ºC). Preliminary kinetics studies indicated that exchange equilibrium in a reference smectite system was achieved in less than 2 hours; the 18 hour reaction time was chosen for convenience. Following the exchange equilibration period, the solution and solid phases were separated by centrifugation and filtration through a 0.45 µm membrane filter and the solution pH was determined. For all experiments, the pH varied between 7.13 and 7.57. The equilibrium solutions were stored under refrigeration until analyzed. The remaining solids were centrifuge washed 3 times with DDI water to remove entrained soluble salts, then washed 3 times with 1.0 M NH_4-acetate (and the supernatant liquid collected) to remove the exchangeable cations. The collected supernatant NH_4-acetate solution was brought to a volume of 100 mL and filtered through qualitative-grade filter paper. The NH_4-acetate extracts were stored in the dark and under refrigeration until analyzed.

2.4 Clay mineralogy and x-ray diffraction

To determine clay mineralogy of the Loring clay separates (15-30 cm and 30-46 cm depths), samples were sequentially treated to remove cementing agents with pH 5.0 ammonium acetate (carbonate removal and Na-saturation), hydrogen peroxide (organic matter and manganese oxide removal), and sodium citrate-bicarbonate-dithionite (iron oxide removal) as described by Jackson (2005). The disaggregated clays were then centrifuge washed 4 times with either 1 M KCl or 1 M $MgCl_2$ and then centrifuge washed 3 times with DDI water to remove entrained soluble salt. Suspensions of K- and Mg-saturated samples were pipetted onto quartz slides and dried overnight at ambient temperature. The slides were then placed in a desiccator over a saturated $MgCl_2$ solution at a relative humidity of 33%. In addition to the ambient temperature K-saturated clay slides, slides were selected for heat treatment in a muffle furnace at

330ºC and 550ºC for 2 hours; these slides were cooled and stored in a desiccator over anhydrite. For the Mg-glycol saturation, an Mg-saturated clay suspension was combined with glycol and the mixture placed on a quartz slide. The Mg-glycol slides were placed in a desiccator over a beaker of glycol and allowed to dry. X-ray diffraction was then preformed to determine *d*-values of the (00*l*) spacings of the layer silicates for the five treatments: K-saturated ambient, K-saturated 330ºC, K-saturated 550ºC, Mg-saturated, and Mg-glycol saturated. X-ray diffractograms were generated using a Bruker Model D8 with Ni-filtered, Cu Kα radiation. The x-ray diffractometer operating parameters were set to 40 kV and 40 mA with a scan range of 2 to 30° 2θ, a step of 0.02 °2θ, and a count rate of 2 seconds per step.

2.5 Analytical

A Hewlett-Packard Series 1100 (Hewlett-Packard Palo Alto, CA) HPLC coupled with UV detection was used to determine Tyl concentrations using a procedure described by Essington et al. (2010) and Lee et al. (2014). An Ascentis C18 guard column (2 cm by 4.0 mm and 5 µm) and an Ascentis C18 analytical column (15 cm by 4.6 mm and 5 µm) with an injection volume of 100 µL and a flow rate of 1 mL min^{-1} was used. The mobile phase was an acetonitrile-0.01 M KH_2PO_4, pH 7.0 gradient ranging from 20:80 to 60:40 in 10 minutes, resulting in a Tyl retention time of 7.8 minutes. A UV detector wavelength of 280 nm results a method detecting limit of 0.008 µmol L^{-1}. The Na and Ca concentrations were determined using a Perkin Elmer AAnalyst 800 atomic absorption spectrophotometer (Wellseley, PA). Sodium was analyzed with emission while Ca with absorbance. The samples and standards were spiked with 12% $LaCl_3$ solution using 0.1 mL for every 10 mL of sample. Sodium and Ca standards were made using atomic absorption standards from CPI International (Springfield, VA). Method detection limits for both Na and Ca were 0.01 mg L^{-1}.

206 A chemical equilibrium modeling program, Visual MINTEQ (VM) (version 3.1) with the
207 built-in NIST 46.7 thermodynamic database (Gustafsson, 2018) was used to compute the free
208 cation concentrations of Na^+, Ca^{2+}, and Tyl^+, as well as their single-ion activities. The database
209 was augmented to include the pK_a value of 7.50 (Qiang and Adams, 2004) for the dissociation of
210 the Tyl dimethylamine functional group. Input data for the speciation model included the
211 equilibrium pH, and the total soluble concentrations of Na or Ca, Tyl, Cl, and tartrate. The
212 concentration of Cl was computed from the Na or Ca content of the blanks, and the concentration
213 of tartrate was computed from the Tyl content of the blanks.

214 *2.6 Infrared spectroscopy*

215 A flow-through, in-situ ATR-FTIR system was used to examine the adsorption of Tyl by
216 the Na- and Ca-saturated soil clays, and by hematite. This system, described in detail by Dolui et
217 al. (2018), consists of a Perkin Elmer Frontier Infrared Spectrometer, a liquid N_2 cooled MCT-A
218 (mercury cadmium telluride) detector, and an optics compartment purged with CO_2- and H_2O-
219 free air. A reaction cell contains a horizontal 45° ZnSe ATR crystal (HATR) (Pike Technologies,
220 Madison, WI) attached to the ATR sample stage of the IR spectrometer. A peristaltic pump
221 (Watson Marlow 400, Falmouth, UK) circulates an Ar-purged solution from a 500-mL solute
222 reservoir through the reaction cell at a rate of 2 mL min^{-1}. The reservoir contains a pH-adjusted,
223 Tyl solution in a 0.01 M NaCl or $CaCl_2$ background electrolyte that is constantly stirred with a
224 magnetic stirring bar. A pH electrode monitors pH in the reservoir during Tyl adsorption.

225 A Na- or Ca-saturated clay or hematite sample (~ 2.5 mg) in 0.01M NaCl or $CaCl_2$ is
226 layered onto the HATR crystal before each ATR-FTIR experiment. The HATR crystal is
227 attached to the ATR sample stage after the mineral film is air-dried overnight. Background FTIR
228 spectra are collected while circulating a pH 7, 0.01 M NaCl or $CaCl_2$ solution over the mineral

film. All subsequent spectra are collected relative to the background. Tylosin is then added to the solute reservoir to yield a circulating solution that is 10 μM Tyl. Spectra are accumulated until the intensity of the IR bands does not change with time. The concentration of Tyl in the reservoir is increased to 100 μM and the accumulation of FTIR spectra is continued until the intensity of the IR bands does not change, which occurs at approximately 4.5 h reaction time. Band assignments were performed according to Amarasinghe et al. (2009) and Yang et al. (2016) (Table S1).

2.7 Exchange data analysis

The concentrations of cations in the exchange phase are directly determined by NH_4 extraction. An exchange isotherm for Tyl is a plot of the equivalent fraction of Tyl^+ on the exchange phase (E_{TylX}, y-axis) versus the equivalent fraction of Tyl^+ in the equilibrium solution (E_{Tyl^+}, x-axis). A detailed description of the development of exchange isotherms is provided by Essington (2015). For NaX-TylX exchange, E_{TylX} is

$$E_{\mathrm{TylX}} = \frac{\{\mathrm{TylX}\}}{\{\mathrm{TylX}\}+\{\mathrm{NaX}\}} \tag{1}$$

where {TylX} and {NaX} are the mol kg^{-1} of Tyl^+ or Na^+ on the exchange phase, and X^- represents a mole of exchange phase charge. Further, the equivalent fraction of Na^+ on the exchange phase is

$$E_{\mathrm{NaX}} = 1 - E_{\mathrm{TylX}} = \frac{\{\mathrm{NaX}\}}{\{\mathrm{TylX}\}+\{\mathrm{NaX}\}} \tag{2}$$

The equivalent fraction of Tyl^+ in solution is

$$E_{\mathrm{Tyl}^+} = \frac{[\mathrm{Tyl}^+]}{[\mathrm{Tyl}^+]+[\mathrm{Na}^+]} \tag{3}$$

and

$$E_{\mathrm{Na}^+} = 1 - E_{\mathrm{Tyl}^+} = \frac{[\mathrm{Na}^+]}{[\mathrm{Tyl}^+]+[\mathrm{Na}^+]} \tag{4}$$

where [Tyl^+] and [Na^+] are the mol L^{-1} of free cation in solution (computed using VM). A similar set of expressions describe the CaX_2-TylX exchange systems:

$$E_{\mathrm{TylX}} = \frac{\{\mathrm{TylX}\}}{\{\mathrm{TylX}\}+2\{\mathrm{CaX_2}\}} \tag{5}$$

$$E_{\mathrm{CaX_2}} = 1 - E_{\mathrm{TylX}} = \frac{2\{\mathrm{CaX_2}\}}{\{\mathrm{TylX}\}+2\{\mathrm{CaX_2}\}} \tag{6}$$

$$E_{\mathrm{Tyl^+}} = \frac{[\mathrm{Tyl^+}]}{[\mathrm{Tyl^+}]+2[\mathrm{Ca^{2+}}]} \tag{7}$$

$$E_{\mathrm{Ca^{2+}}} = 1 - E_{\mathrm{Tyl^+}} = \frac{2[\mathrm{Ca^{2+}}]}{[\mathrm{Tyl^+}]+2[\mathrm{Ca^{2+}}]} \tag{8}$$

Also plotted on the exchange isotherm is the non-preference isotherm, obtained from Essington (2015). For NaX-TylX exchange, the non-preference isotherm is $E_{\mathrm{TylX}} = E_{\mathrm{Tyl^+}}$. For CaX_2-TylX exchange, the non-preference isotherm is

$$E_{\mathrm{TylX}} = \left\{1 + \frac{2}{\Gamma\, N_{\mathrm{T}}}\left[\frac{1}{E^2_{\mathrm{Tyl^+}}} - \frac{1}{E_{\mathrm{Tyl^+}}}\right]\right\}^{-0.5} \tag{9}$$

where N_T is the total normality, $\Gamma = \frac{\gamma^2_{\mathrm{Tyl^+}}}{\gamma_{\mathrm{Ca^{2+}}}}$, and the γ's are single-ion activity coefficients. The non-preference isotherm describes the condition where neither cation is preferred by the exchange phase. The non-preference condition is met when the Vanselow selectivity coefficient (K_V) for the exchange reaction is unity. For the NaX + Tyl^+ = TylX + Na^+ exchange reaction, K_V is

$$K_{\mathrm{V}} = \frac{N_{\mathrm{TylX}}(\mathrm{Na^+})}{N_{\mathrm{NaX}}\,(\mathrm{Tyl^+})} \tag{10}$$

For the CaX_2 + 2Tyl^+ = 2TylX + Ca^{2+} exchange reaction, K_V is

$$K_{\mathrm{V}} = \frac{N^2_{\mathrm{TylX}}(\mathrm{Ca^{2+}})}{N_{\mathrm{CaX_2}}(\mathrm{Tyl^+})^2} \tag{11}$$

In Eqs. (10) and (11) the parentheses represent activity (obtained from VM) and N_{TylX}, N_{NaX}, and $N_{\mathrm{CaX_2}}$, are the mole fractions:

$$N_{\mathrm{TylX}} = \frac{\{\mathrm{TylX}\}}{\{\mathrm{TylX}\}+\{\mathrm{NaX}\}} \; ; N_{\mathrm{NaX}} = 1 - N_{\mathrm{TylX}} = \frac{\{\mathrm{NaX}\}}{\{\mathrm{TylX}\}+\{\mathrm{NaX}\}} \tag{12}$$

$$N_{\mathrm{TylX}} = \frac{\{\mathrm{TylX}\}}{\{\mathrm{TylX}\}+\{\mathrm{CaX_2}\}}; N_{\mathrm{CaX_2}} = 1 - N_{\mathrm{TylX}} = \frac{\{\mathrm{CaX_2}\}}{\{\mathrm{TylX}\}+\{\mathrm{CaX_2}\}} \tag{13}$$

A plot of ln K_{V} [Eqs. (10) or (11)] as a function of E_{TylX} [Eqs. (1) or (5)] provides a mechanism to determine the true exchange equilibrium constant (K_{ex}) (Essington, 2015).

A mass balance was performed to determine the nonexchangeable concentration of adsorbed Tyl. For initially Na- or Ca-saturated samples, the mass of Tyl added to the suspensions is determined from the blanks. The mass balance expression for adsorbed Tyl is: ${}^{\mathrm{Tyl}}n_{\mathrm{T}} = {}^{\mathrm{Tyl}}n_{\mathrm{ex}} + {}^{\mathrm{Tyl}}n_{\mathrm{nonex}}$, where ${}^{\mathrm{Tyl}}n_{\mathrm{T}}$ represents the total mass of adsorbed Tyl determined by subtracting the mass of Tyl in the equilibrium suspensions from that added; ${}^{\mathrm{Tyl}}n_{\mathrm{ex}}$ is directly measured and represents the exchangeable mass of adsorbed Tyl; and ${}^{\mathrm{Tyl}}n_{\mathrm{nonex}}$ is determined by difference and represents the nonexchangeable forms of adsorbed Tyl. The adsorbed Tyl concentration of any one of the adsorbed Tyl components is obtained by dividing n values by the mass of soil. For example, the total surface excess of adsorbed Tyl (in mmol kg^{-1}) is $q_{\mathrm{T}} = {}^{\mathrm{Tyl}}n_{\mathrm{T}}/m_{\mathrm{S}}$, where m_{S} is the mass of the adsorbant in kg. Adsorption isotherms were generated for total adsorbed and exchangeable Tyl. An adsorption isotherm is a plot of the amount of Tyl adsorbed by the surface (e.g., q_{T}, y-axis) versus the total concentration of Tyl in the equilibrium solution (C_{eq} in mmol L^{-1}, x-axis). The isotherms were described using the constant partition equation, $q_{\mathrm{T}} = K_{\mathrm{P}}C_{\mathrm{eq}}$, where K_{P} is the partition constant obtained using least square linear regression analysis.

3. Results and discussion

3.1 Clay mineralogy

The adsorption capacity of soil for Tyl, and the distribution of adsorbed Tyl into exchangeable and nonexchangeable forms, is dictated to a large degree by the clay mineralogy (Bewick, 1979; Call et al., 2019). The adsorption of Tyl by non-expansive clay minerals (e.g., the micas and kaolinite) and partially expansive vermiculites is restricted to the external surfaces, while Tyl can intercalate the smectites, generating high adsorption capacities. The cation saturations and heat treatments imposed on the soil size clay fraction of the Loring Bt horizons provide a Group level characterization of the common soil phyllosilicates. The subsoil horizons of the Loring soil display similar clay mineralogy (Fig. 2). The 1.47 nm diffraction in the Mg-saturated samples shifts to approximately 1.7 nm upon glycolation; this is diagnostic for the occurrence of smectite. The 1.0 nm diffraction in the Mg- and Mg glycol-saturated samples is indicative of the presence of mica, while the diffraction at > 2.0 nm indicates the occurrence of an interstratified mica-smectite. The disappearance of the 0.72 nm diffraction upon heating to 550°C indicates kaolinite. The remaining diffractions are second order mica (0.5 nm) and kaolinite (0.36 nm), and third order mica (0.33) or quartz. Thus, the clay mineral assemblage in the Loring subsoil consists of mica, smectite, mica-smectite interstratification, and kaolinite.

3.2 Binary exchange isotherms

For the NaX-TylX exchange systems, the exchange isotherms illustrate little preference for Tyl^+ or Na^+ by the exchange phase in the subsurface horizons (Fig. 3a). However, Na^+ is preferred relative to Tyl^+ in Bt1 systems when the clays are initially Tyl-saturated, and when $E_{TylX} > 0.25$. When initially Na-saturated, K_V values for NaX→TylX exchange [Eq. (10)] do not vary with exchange phase composition, averaging 1.12 ± 0.20 for Bt1 and 1.41 ± 0.24 for Bt2 within the E_{TylX} range studied (Fig. 4a). On average, there is no preference of Tyl^+ over Na^+ for the exchange phase when the clays are initially Na-saturated, as the K_V values are not

significantly different from unity. When initially Tyl-saturated, Tyl^+ is preferred over Na^+ at low E_{TylX} values; K_V is 3.95 ± 0.51 when E_{TylX} = 0.08 in Bt1, and 3.91 ± 0.72 when E_{TylX} is 0.21 in Bt2. However, K_V values decrease with increasing E_{TylX}, achieving constant values of 0.79 ± 0.29 for Bt1 and 1.18 ± 0.32 when E_{TylX} > 0.25 (which are also not significantly different from unity). The soil clay minerals are less selective for Tyl^+ over Na^+ than STx-1 reference montmorillonite (Call et al., 2019). They observed a mean K_V value of 6.61 ± 2.62 when E_{TylX} ranged between 0.09 and 0.85. Tylosin is also less competitive with Na^+ than other monovalent cations in smectites and smectitic soils. Vanselow selectivity coefficients evaluated when E_{NaX} = 0.5 range from 1.74 to 6.23 for NaX→KX, 3.54 to 20.6 for NaX→RbX, and 7.1 to 121 for NaX→CsX exchange (Deist and Talibudeen, 1967; Gast, 1972; Jensen and Babcock, 1973; Xu and Harsh, 1990; Tournassat et al., 2009).

In the CaX_2-TylX exchange systems, CaX_2 dominates the exchange phase. However, Tyl^+ is preferred because there is greater TylX then predicted by the nonpreference isotherm when E_{TylX} < 0.2 (Fig. 3b). The K_V values for the CaX_2→TylX exchange reaction [Eq. (11)] vary as a function of E_{TylX} (Fig. 4b). When initially Ca-saturated, K_V decreases from 17. 6 to 3.44 as E_{TylX} increases from 0.01 to 0.08 in Bt1, and from 58.1 to 6.28 as E_{TylX} increases from 0.02 to 0.14 in Bt2. This trend is similar for initially Tyl-saturated clay, as K_V decreases from 6.14 to 1.34 as E_{TylX} increases from 0.09 to 0.40 in Bt1, and from 21.6 to 1.67 as E_{TylX} increases from 0.14 to 0.36 in Bt2. In general, K_V values for CaX_2→TylX exchange are greater in Bt2 relative to Bt1. The preference of the soil clay for Tyl^+ over Ca^{2+}, and the decreasing preference with increasing E_{TylX} is similar to that observed for CaX_2→TylX exchange on STx-1 montmorillonite (Call et al., 2019). They observed K_V values to decrease from 388 to ~1 when E_{TylX} increased from 0.02 to 0.40. For smectites and smectitic soils, K_V values for Na^+ and K^+ exchange with Ca^{2+} also

decrease with increasing E_{NaX} and E_{KX}. When E_{NaX} = 0.5, K_V values for $CaX_2 \rightarrow NaX$ exchange range from 0.15 to ~1 (Rytwo et al., 1996; Sposito et al., 1983; Tournasset et al., 2009). When E_{KX} = 0.5, K_V values for $CaX_2 \rightarrow KX$ exchange range from 2.24 to 22.2 (Deist and Talibudeen, 1967; Jensen and Babcock, 1973; Evangelou, 1998; Essington, 2015; Ritter et al., 2017). These comparison indicate that Tyl^+ is less competitive than K^+ in exchange with CaX_2, but that Tyl^+ and Na^+ have similar selectivity.

3.3 Cation exchange capacity

The *CEC* values of the Bt1 and Bt2 clays measured by Ca-NH_4 acetate exchange were 43.9 ± 1.87 and 36.1 ± 1.91 $cmol_c\ kg^{-1}$. However, the *CEC* in the binary exchange systems, determined by the summation of exchangeable cation charge, also varied as a function of the initial saturating cation. For the Bt1 NaX-TylX systems that were initially Na-saturated, the *CEC* was 10.3 ± 1.60 $cmol_c\ kg^{-1}$. When initially Tyl-saturated, the *CEC* was 3.45 ± 0.33 $cmol_c\ kg^{-1}$. The *CEC* was also depressed in the Bt2 NaX-TylX systems: 15.9 ± 1.80 $cmol_c\ kg^{-1}$ when initially Na-saturated, and 4.81 ± 0.43 $cmol_c\ kg^{-1}$ when Tyl-saturated. The *CEC* values in the initially Ca-saturated CaX_2-TylX exchange systems were similar to those determined by Ca-NH_4 acetate exchange; 46.6 ± 3.34 $cmol_c\ kg^{-1}$ for Bt1 and 37.3 ± 1.32 $cmol_c\ kg^{-1}$ for Bt2. However, when initially Tyl-saturated, the *CEC* values were 4.50 ± 1.47 $cmol_c\ kg^{-1}$ for Bt1 and 6.99 ± 1.44 $cmol_c\ kg^{-1}$ for Bt2.

The reduction in *CEC* associated with Tyl retention was also observed in montmorillonite systems (Call et al., 2019). These authors postulated that due to its size, intercalated Tyl was blocking the access of cations to the exchange locations. Ivanov (1998, 2002), using molecular mechanics modeling techniques, determined that Tyl in solutions may exist in two configurations: an unfolded linear structure was predicted to be the most stable, while a less

stable folded structure was also predicted. Call et al. (2019) reported the approximate solvent-accessible dimensions of the linear structure were 2.71 nm × 0.95 nm × 1.47 nm, while those of the folded structure were 2.71 nm × 1.47 nm × 1.35 nm. For an example montmorillonite with a unit cell layer charge of 1.12 and unit cell *a* and *b* dimensions of 0.52 nm and 0.9 nm, the surface area per unit charge is 0.84 nm^2/z. If viewed as a box-like structure, the area of the Tyl molecule sides in the linear configuration are 4.0 nm^2, 2.6 nm^2, and 1.4 nm^2; those for the folded configuration are 3.1 nm^2, 2.9 nm^2, and 2.0 nm^2. All of these exceed the area associated with unit charge in a smectite interlayer, indicating that blocking the access of cations to exchange locations by Tyl reduces the apparent *CEC* of the adsorbent.

3.4 Adsorption isotherms

The adsorption isotherms indicate that the total adsorption of Tyl is influenced by the horizon and the competing cation (Fig. 5). There is significantly greater adsorption in Bt2 relative to Bt1 in both the NaX-TylX and CaX_2-TylX systems, as quantified by the linear partition coefficients (Table 1). There is also greater Tyl retention in the NaX-TylX systems relative to the CaX_2-TylX systems, a finding that is consistent with that of prior research (Bewick, 1979; Essington et al., 2010; Lee et al., 2014). The fraction of the total adsorbed Tyl that is exchangeable also varies with horizon and competing cation. Approximately 36% of adsorbed Tyl is exchangeable in the Bt1, NaX-TylX systems, compared to 43% in Bt2. In the CaX_2-TylX systems, 57% of the total adsorbed Tyl is exchangeable in Bt1, 66% in Bt2.

There is also very little difference between exchangeable Tyl in the Na- and Ca-dominated systems in Bt1 (Fig. 5, Table 1), although there is significantly greater exchangeable Tyl in the Na-systems in Bt2. The *CEC* of the CaX_2-TylX systems (46.6 $cmol_c\ kg^{-1}$ for Bt1 and 37.3 $cmol_c\ kg^{-1}$ for Bt2) is significantly greater than that of the NaX-TylX systems (10.2 $cmol_c$

kg^{-1} for Bt1 and 15.9 cmol$_c$ kg^{-1} for Bt2). However, E_{TylX} only ranges up to approximately 0.1 for CaX_2-TylX exchange, but ranges up to 0.4 in NaX-TylX. Thus, the surface excess of exchangeable Tyl are similar between the Ca- and Na systems. The nonexchangeable component of adsorbed Tyl is greater in the Na-systems, with K_P values of 21.8 and 33.4 for Bt1 and Bt2, relative to the Ca-systems (K_P values of approximately 8 for both horizons) (Table 1).

3.5 Infrared spectroscopy

The sharp increase in IR band intensity at 1588 cm^{-1} (Fig. 6a and b) indicates the possible bonding of Tyl on mineral surfaces through the dimethylamine [–N(CH$_3$)$_2$] functional group. Bands at 1580-1590 cm^{-1} are due to the N-H bending vibrations. Coupled with this is the strong IR band at 1385 cm^{-1} and the weaker bands at 1458 cm^{-1} and 1320 cm^{-1}, which represent the C-H bending vibrations of the dimethylamine (Amarasinghe et al., 2009). Conversely, the 1390-1310 cm^{-1} region may also represent the O-H vibrations from phenols. The shoulder bands at 1712 and 1661 cm^{-1} are most likely due to the interactions of the aromatic aldehyde (–CHO) and carbonyl (–C=O) groups with the mineral surfaces. Interestingly, in the $CaCl_2$ medium, the IR band a near 1580-1590 cm^{-1} appeared as a shoulder to the more pronounced 1627 cm^{-1} band (Fig. 6b). A broad IR band near 1627 cm^{-1} and a shoulder at 1659 cm^{-1} are features that differ from the IR spectra collected in the NaCl medium. The salt effect on these IR bands may indicate an outer-sphere adsorption mechanism through the electronegative carbonyl moieties and positive surface sites.

The IR bands at 1077, 1029-1031, 1001-1011 cm^{-1} (Figs. 6a and b) have been identified as γ(Si-O) vibration bands that represent the interlayer adsorption of highly polar molecules by phyllosilicates (Amarasinghe et el., 2009; Yang et al., 2016). Call et al., (2019) observed these bands to predominate the IR spectra of Tyl adsorbed by montmorillonite from both NaCl and

$CaCl_2$ media. Correspondingly, they also observed the direct intercalation of Tyl into the montmorillonite interlayers. Other IR bands found in the montmorillonite systems (1590, 1462, 1383, 1317, and 1163 cm^{-1}), which represent H-bonding, surface interactions through the dimethylamine, and internal ring vibrations of the Tyl molecule were minor, indicating only the minor covalent and external surface bonding of Tyl. By comparison, the intense IR bands in the 1590-1720 cm^{-1} range indirectly support the hypothesis that the Tyl functional groups primarily interact through covalent bonding with the external surfaces of the soil minerals. Further, only approximately 36% to 43% of the adsorbed Tyl is exchangeable in NaCl systems, and 57% to 66% in $CaCl_2$, supporting the significance of Tyl adsorption on the external clay surfaces, as well as other soil minerals. To test this hypothesis, the IR spectra of Tyl adsorbed by hematite was examined (Fig. 6c). The iron oxide content of the Loring soil 15-30 cm and 30-46 cm depth increments is approximately 2 to 3% (unpublished data); thus, hematite is a surrogate for the soil iron oxides. The strong IR bands near 1586 cm^{-1} and 1387 cm^{-1}, with weaker bands in the 1334-1310 cm^{-1} range, are similar to the band locations for the Tyl-soil interactions, suggesting similar bonding mechanisms. Further, IR bands near 1139, 1084, and 1000 cm^{-1}, which were identified as γ(Si-O) vibration bands, also appear in the hematite spectra. It is possible some overlapping IR bands from H-bonding, ring-OH groups, and internal ring vibrations of the Tyl molecule also appear in this region. Overall, the IR bands from Tyl-soil and Tyl-hematite interactions, coupled with the significant distribution of adsorbed Tyl into non-exchangeable forms (Fig. 5), suggest that adsorption on external phyllosilicate and iron oxide surfaces are important retention mechanisms, possibly through carbonyl and dimethylamine moieties, with minor phyllosilicate interlayer adsorption.

4. Conclusions

The adsorbed Tyl in pH neutral, smectitic subsoil horizons is divided into exchangeable and nonexchangeable forms. The percentage of adsorbed Tyl that is exchangeable varies from 36% to 43% when Na^+ is the competing cation, and from 57% to 66% when Ca^{2+} competes. Thus, cation exchange is an important mechanism for the retention of Tyl by the soil clay fraction. In NaX-TylX binary exchange systems, neither Na^+ nor Tyl^+ is preferred by the clay exchange phase, and the Vanselow selectivity coefficients (K_V) for the NaX→TylX exchange reaction range between 0.79 and 1.41. In addition, K_V is generally invariant with exchange phase composition. In the CaX_2-TylX systems, Tyl^+ is preferred by the clay exchange phase when the equivalent fraction of TylX (E_{TylX}) is less than 0.4. The K_V values for the CaX_2→TylX exchange reaction are at a maximum at the lowest E_{TylX} values, with $17.6 < K_V < 58.1$, then decrease with increasing E_{TylX} to $1.34 < K_V < 6.28$. Adsorbed Tyl masks the *CEC* of the soil clays; the effect was greatest in systems that were initially Tyl-saturated. However, this effect was also apparent to the lowest levels of TylX ($E_{TylX} < 0.01$), and was attributed to the steric effects of the large Tyl molecule. The *in-situ* ATR-FTIR spectra indicate that surface interactions of Tyl with soil iron oxides, through the dimethylamine functional group, may be an important retention mechanism. The findings of this study directly illustrate the importance of ion exchange as a mechanism for the retention of Tyl in soil, and provide a molecular-level characterization of the surface complexation of Tyl in soil.

Acknowledgements

Financial support of this research by USDA-NIFA project number TEN00476 is gratefully acknowledged.

References

Allaire, S.E., Del Castillo, J., Juneau, V. 2006. Sorption kinetics of chlortetracycline and tylosin on sandy loam and heavy clay soils. J. Environ. Qual. 35, 969-972.

Amarasinghe, P.M., Katti, K.S., Katti, D.R. 2009. Nature of organic fluid-montmorillonite interactions: an FTIR spectroscopic study. J. Colloid Interface Sci. 337, 97-105.

Bewick, M.W.M. 1979. The adsorption and release of tylosin by clays and soils. Plant Soil 51, 363-372.

Call, J.J., Rakshit, S., Essington, M.E. 2019. The adsorption of tylosin by montmorillonite and vermiculite: exchange selectivity and intercalation. Soil Sci. Soc. Am. J. doi:10.2136/sssaj2018.12.0475.

Chander, Y., Kumar, K., Goyal, S.M., Gupta, S.C. 2005. Antibacterial activity of soil-bound antibiotics. J. Environ. Qual. 34, 1952-1957.

Deist, J., Talibudeen, O. 1967. Ion exchange in soils from the pairs K-Ca, K-Rb, and K-Na. J. Soil Sci. 18, 125-137.

Dolui, M., Rakshit, S., Essington, M.E., Lefèvre, G. 2018. Probing oxytetracycline sorption mechanism on kaolinite in a single ion and binary mixtures with phosphate using in situ ATR-FTIR spectroscopy. Soil Sci. Soc. Am. J. 82, 826-838.

Dungan, R.S., Snow, D.D., Bjorneberg, D.L. 2017. Occurrence of antibiotics in an agricultural watershed in south-central Idaho. J. Environ. Qual. 46, 1455-1461.

Essington, M.E. 2015. Soil and Water Chemistry: An Integrative Approach, second ed. CRC press, Boca Raton, FL.

Essington, M. E., J. Lee, J., Seo, Y. 2010. Adsorption of antibiotics by montmorillonite and kaolinite. Soil Sci. Soc. Am. J. 74, 1577-1588.

473 Evangelou, V.P. 1998. Environmental Soil and Water Chemistry: Principles and Applications, J.
474 Wiley & Sons, New York.
475 Fish, B.J., Carr, G.P.R. 1986. Pharmacopoeial procedure for the determination of tylosin factors
476 by high-performance liquid chromatography. J. Chromatography 353, 39-50.
477 Gast, R.G. 1972. Alkali metal cation exchange on Chambers montmorillonite. Soil Sci. Soc. Am.
478 J. 36, 14-19.
479 Gustafsson, J.P. 2018. Visual MINTEQ. Version 3.1. Stockholm: KTH Royal Institute of
480 Technology. http://vminteq.lwr.kth.se/.
481 Hamill, R.L., Haney, M.E., Stamper, M., Wiley, P.F. 1961. Tylosin, a new antibiotic. II.
482 Isolation, properties, and preparation of desmycosin, a microbiological active degradation
483 product. Antibiot. Chemother. 11, 328-334.
484 Ivanov, P.M. 1998. Molecular mechanics conformational analysis of tylosin. J. Molecular
485 Structure 440, 121-130.
486 Ivanov, P.M. 2002. CONFLEX/MM3 search/minimization study of the conformations of the
487 macrolide tylosin. J. Molecular Structure 606, 217-229.
488 Jackson, M.L. 2005. Soil Chemical Analysis-Advanced Course, second ed. University of
489 Wisconsin-Madison Libraries, Madison, WI.
490 Jagadamma, S., Essington, M.E., Xu, S., Yin, X. 2019. Total and active soil organic carbon from
491 long-term agricultural management practices in West Tennessee. Agric. Environ. Letters.
492 doi: 10.2134/ael2018.11.0062.
493 Jensen, H.E., Babcock, K.L. 1973. Cation-exchange equilibria on a Yolo loam. Hilgardia 41,
494 475-488.

495 Joy, S.R., Bartelt-Hunt, S.L., Snow, D.D., Gilley, J.E., Woodbury, B.L., Parker, D.B., Marx,
496 D.B., Li, X. Fate and transport of antimicrobials and antimicrobial resistance genes in soil
497 and runoff following land application of swine manure slurry. Environ. Sci. Technol. 47,
498 12081-12088.
499 Kumar, K., Gupta, S.C., Chander, Y., Singh, A.K. 2005. Antibiotic use in agriculture and its
500 impact on the terrestrial environment. Adv. Agron. 87.
501 Lee, J., Seo, Y., Essington, M.E.. 2014. Sorption and transport of veterinary pharmaceuticals in
502 soil - a laboratory study. Soil Sci. Soc. Am. J. 78, 1531-1543.
503 Lindbo, D.L., Rhoton, F.E., Bigham, J.M., Jones, F.S., Smeck, N.E., Hudnall, W.H., Tyler, D.D.
504 1994. Bulk density and fragipan identification in loess soils of the lower Mississippi River
505 valley. Soil Sci. Soc. Am. J. 58, 884-891.
506 Loke, M.L., Tjørnelund, J., Halling-Sørensen, B. 2002. Determination of the distribution
507 coefficient (log K_d) of oxytetracycline, tylosin A, olaquindox and metronidazole in manure.
508 Chemosphere 48, 351-361.
509 Luby, E.M., Moorman, T.B., Soupir, M. 2016. Fate and transport of tylosin-resistant bacteria and
510 macrolide resistant genes in artificially drained agricultural fields receiving swine manure.
511 Sci. Total Environ. 550, 1126-1133.
512 McFarland, J.W., Berger, C.M., Froshauer, S.A., Hayashi, S.F., Hecker, S.J., Jaynes, B.H.,
513 Jefson, M.R., Kamicker, B.J., Lipinski, C.A., Lundy, K.M., Reese, C.P., Vu, C.B. 1997.
514 Quantitative structure-activity relationships among macrolide antibacterial agents: in vitro
515 and in vivo potency against *Pasteurella multocida*. J. Med. Chem. 40, 1340-1346.
516 Qiang, Z., Adams, C. 2004. Potentiometric determination of acid dissociation constants (pK_a) for
517 human and veterinary antibiotics. Water Res. 38, 2874-2890.

518 Rabølle, M., Spliid, N.H. 2000. Sorption and mobility of metronidazole, olaquindox,
519 oxytetracycline and tylosin in soil. Chemosphere 40, 715-722.
520 Rakshit, S., Sallman, B., Davantés, A., Lefèvre, G. 2017. Tungstate (VI) sorption on hematite: an
521 *in situ* ATR-FTIR probe on the mechanism. Chemosphere 168,685-691.
522 Ritter, S., DeSutter, T., O'Brien, P., Casey, F., Wick, A., Horsager, K., Khan, E. 2017. Binary
523 exchanges of calcium, magnesium, and potassium on thermally desorbed soil. Soil Sci.
524 Soc. Am. J. 81, 1088-1095.
525 Rytwo, G., Banin, A., Nir, S. 1996. Exchange reactions in the Ca-Mg-Na-montmorillonite
526 system. Clays Clay Miner. 44, 276-285.
527 Sallman, B., Rakshit, S., Lefèvre, G. 2018. Influence of phosphate on tungstate sorption on
528 hematite: a macroscopic and spectroscopic evaluation of the mechanism. Chemosphere
529 213,596-601.
530 Sassman, S.A., Sarmah, A.K., Lee, L.S. 2007. Sorption of tylosin A, D, and A-aldol and
531 degradation of tylosin A in soils. Environ. Toxicol. Chem. 26, 1629-1635.
532 Soni, B., Bartelt-Hunt, S.L., Snow, D.D., Gilley, J.E., Woodbury, B.L., Marx, D.B., Li, X. 2015.
533 Narrow grass hedges reduce tylosin and associated antimicrobial resistance genes in
534 agricultural runoff. J. Environ. Sci. 44, 895-902.
535 Sposito, G., Jouany, C., Holtzclaw, K.M., LeVesque C.S. 1983. Calcium-magnesium exchange
536 on Wyoming bentonite in the presence of adsorbed sodium. Soil Sci. Soc. Am. J. 47, 1081-
537 1085.
538 Srinivasan, P., Sarmah, A.K., Manley-Harris, M. 2014. Sorption of selected veterinary
539 antibiotics onto dairy farming soils of contrasting nature. Sci. Total Environ. 472, 695-703.

540 Stromer, B.S., Woodbury, B., Williams, C.F. 2018. Tylosin sorption to diatomaceous earth
541 described by Langmuir isotherm and Freundlich isotherm models. Chemosphere 193, 912-
542 920.
543 Sura, S., Degenhardt, D., Cessna, A.J., Larney, F.J., Olson, A.F., McAllister, T.A. 2016.
544 Transport of three antimicrobials in runoff from windrows of composted beef cattle
545 manure. J. Environ. Qual. 45, 494-502.
546 ter Laak, T.L., Gebbink, W.A., Tolls, J. 2006. The effect of pH and ionic strength on the sorption
547 of sulfachloropyridazine, tylosin, and oxytetracycline to soil. Environ. Toxicol. Chem. 25,
548 904-911.
549 Tournassat, C., Gailanou, H., Crouzet, C., Braibant, G., Gautier, A., Gaucher, E.C. 2009. Cation
550 exchange selectivity coefficient values on smectite and mixed-layer illite/smectite minerals.
551 Soil Sci. Soc. Am. J. 73, 928-942.
552 Wollenberger, L., B. Halling-Sørensen, K.O. Kusk. 2000. Acute and chronic toxicity of
553 veterinary antibiotics to *Daphnia magna*. Chemosphere 40:723-730.
554 Xu, S., Harsh, J.B. 1990. Hard and soft acid-base model verified for monovalent cation
555 selectivity. Soil Sci. Soc. Am. J. 54, 1596-1601.
556 Yang, Y., Wang, S., Liu, J., Xu, Y., Zhou, X. 2016. Adsorption of lysine on Na-montmorillonite
557 and competition with Ca^{2+}: a combined XRD and ATR-FTIR study. Langmuir 32,4746-
558 4754.
559 Zhang, Q., Yang, C., Huang, W., Dang, Z., Shu, X. 2013. Sorption of tylosin on clay minerals.
560 Chemosphere 93, 2180-2186.
561

List of Figures

Figure 1. The structure of tylosin.

Figure 2. X-ray diffractograms of (a) Bt1 and (b) Bt2 horizons of the Loring soil. A: Mg^{2+}-saturated; B: Mg^{2+}-glycol-saturated; C: K^{+}-saturated ambient temperature; D: K^{+}-saturated 330°C; E: K^{+}-saturated 550°C. Diffractions are identified by their *d*-values in nm.

Figure 3. Exchange isotherms for the binary (a) NaX-TylX and (b) CaX_2-TylX systems that illustrate the equivalent fraction of tylosin on the exchange phase (E_{TylX}) as a function of the equivalent fraction of tylosin in solution (E_{Tyl^+}), initial cation saturation, and soil horizon. The solid line represents the non-preference (NP) line.

Figure 4. The variation of the Vanselow selectivity coefficient [(as ln K_V), Eqs. (10) and (11)] in (a) Bt1 and (b) Bt2 horizons as a function of the equivalent fraction of tylosin on the exchange phase (E_{TylX}) and initial cation saturation.

Figure 5. Total and exchangeable tylosin adsorption isotherms in (a) Bt1 and (b) Bt2 horizons. The lines represent the linear partition model (Table 1); q_{Tyl} and C_{eq} are the equilibrium surface excess and the solution concentration of tylosin.

Figure 6. Growth of in-situ ATR-FTIR bands upon tylosin adsorption by Bt2 (15-30 cm) horizon from (a) 0.01 M NaCl and (b) 0.01 M $CaCl_2$ solutions. The spectra in (c) represents tylosin adsorption by hematite from 0.01 M NaCl. [color online]

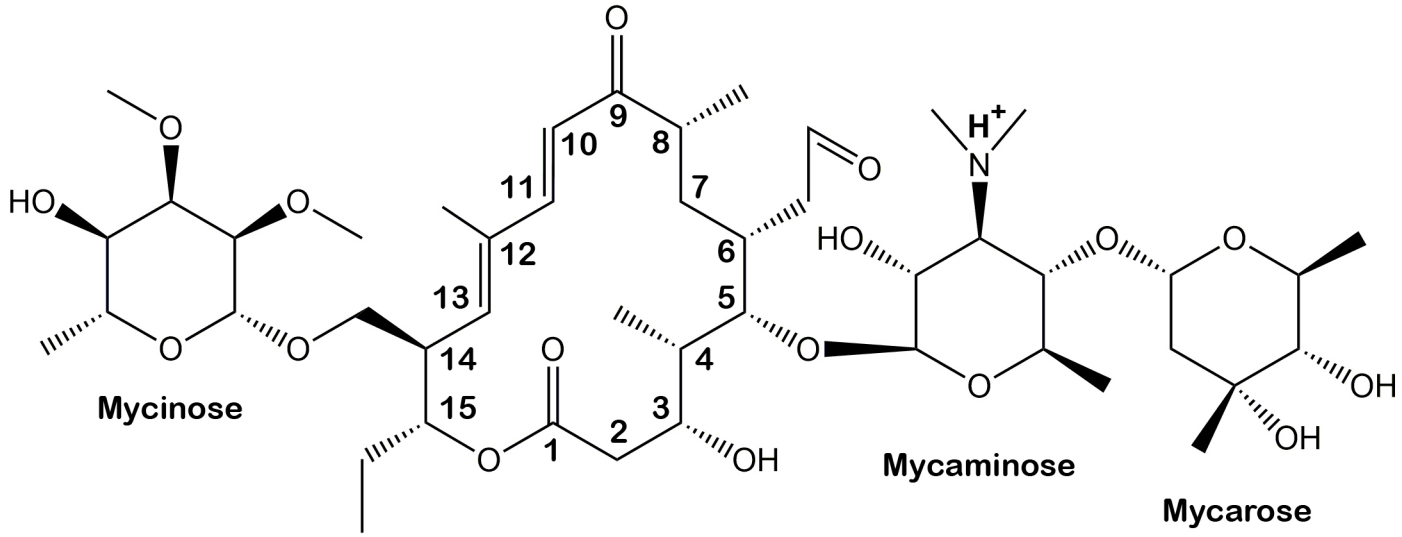
Mycinose
Mycaminose
Mycarose

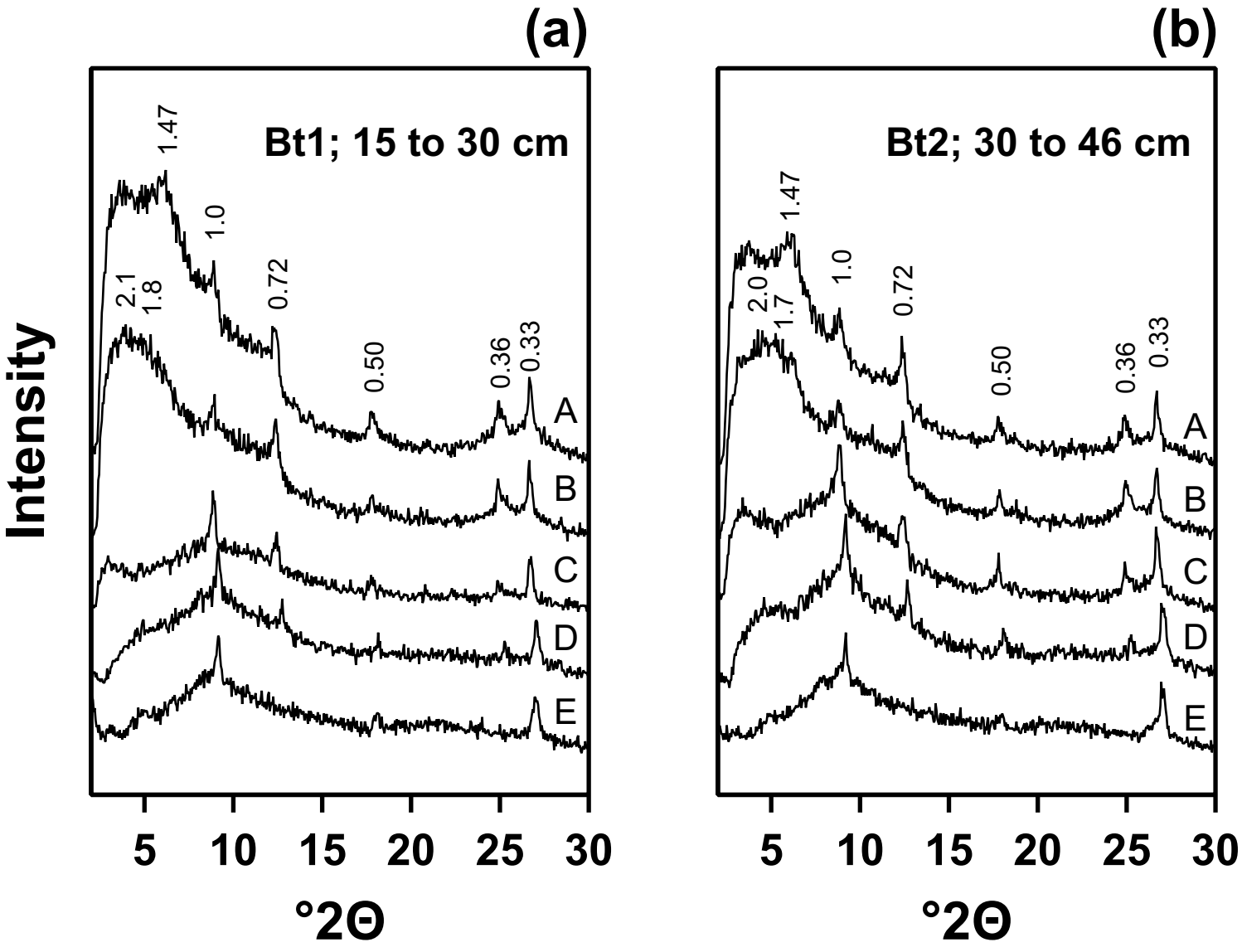
(a)
Bt1; 15 to 30 cm
1.47
1.0
2.1
1.8
0.72
0.50
0.36
0.33
A
B
C
D
E
Intensity
5
10
15
20
25
30
°2Θ
(b)
Bt2; 30 to 46 cm
1.47
2.0
1.7
1.0
0.72
0.50
0.36
0.33
A
B
C
D
E
5
10
15
20
25
30
°2Θ

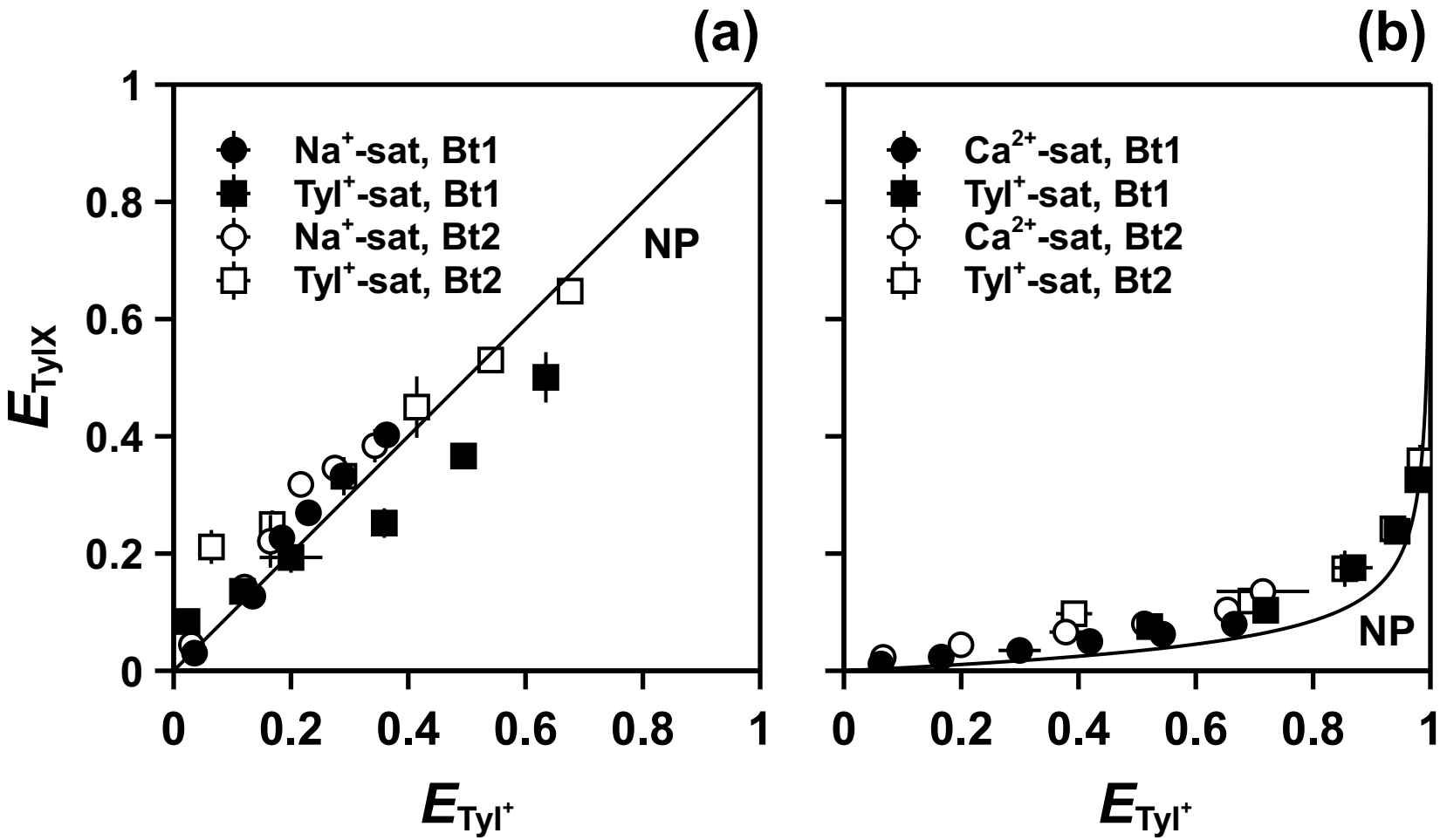
(a)
(b)
Na+-sat, Bt1
Tyl+-sat, Bt1
Na+-sat, Bt2
Tyl+-sat, Bt2
NP
Ca2+-sat, Bt1
Tyl+-sat, Bt1
Ca2+-sat, Bt2
Tyl+-sat, Bt2
NP
ETylX
ETyl+
ETyl+
0
0.2
0.4
0.6
0.8
1

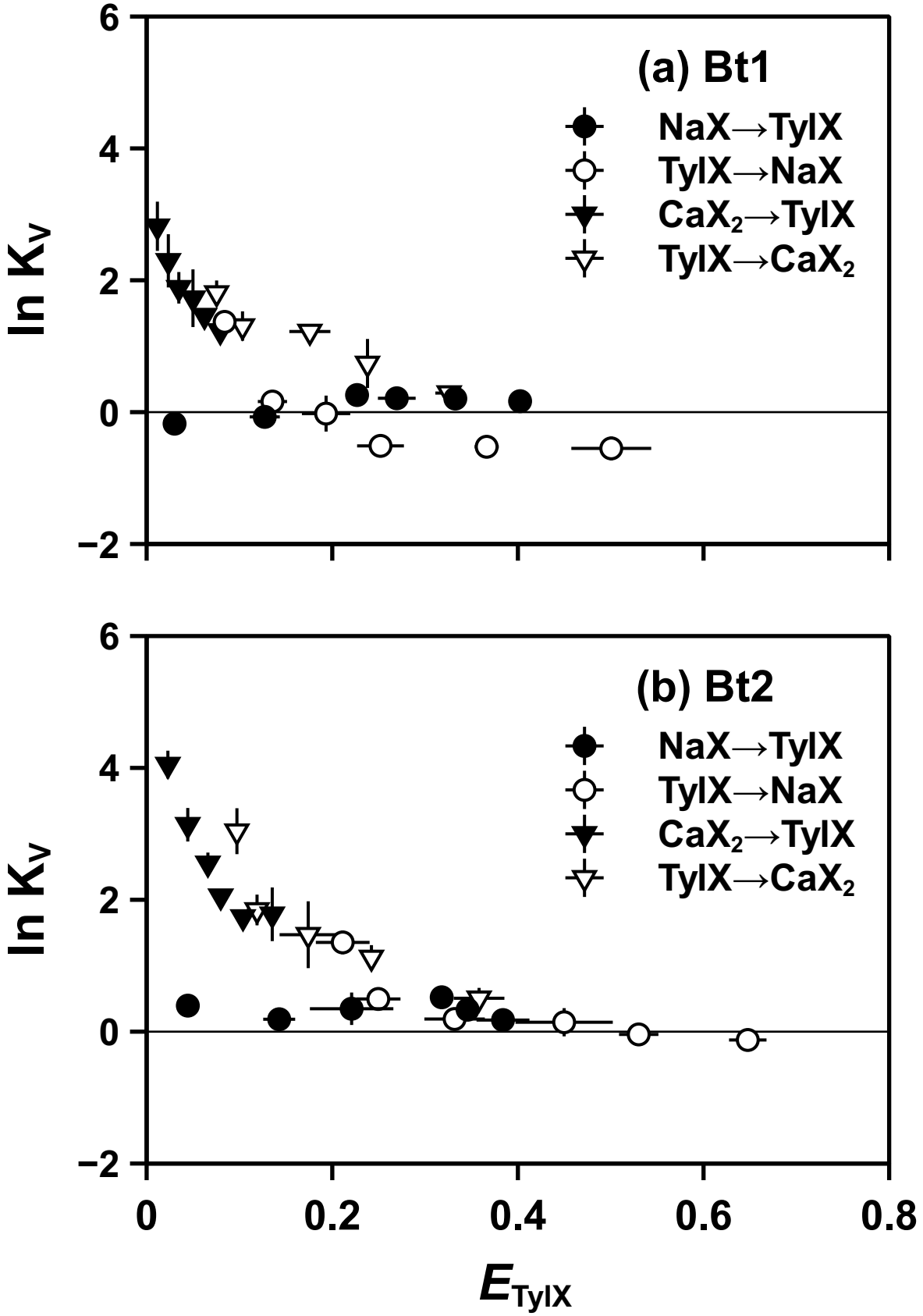
(a) Bt1
NaX→TylX
TylX→NaX
CaX2→TylX
TylX→CaX2
ln Kv
6
4
2
0
−2
(b) Bt2
NaX→TylX
TylX→NaX
CaX2→TylX
TylX→CaX2
ln Kv
6
4
2
0
−2
0
0.2
0.4
0.6
0.8
ETylX

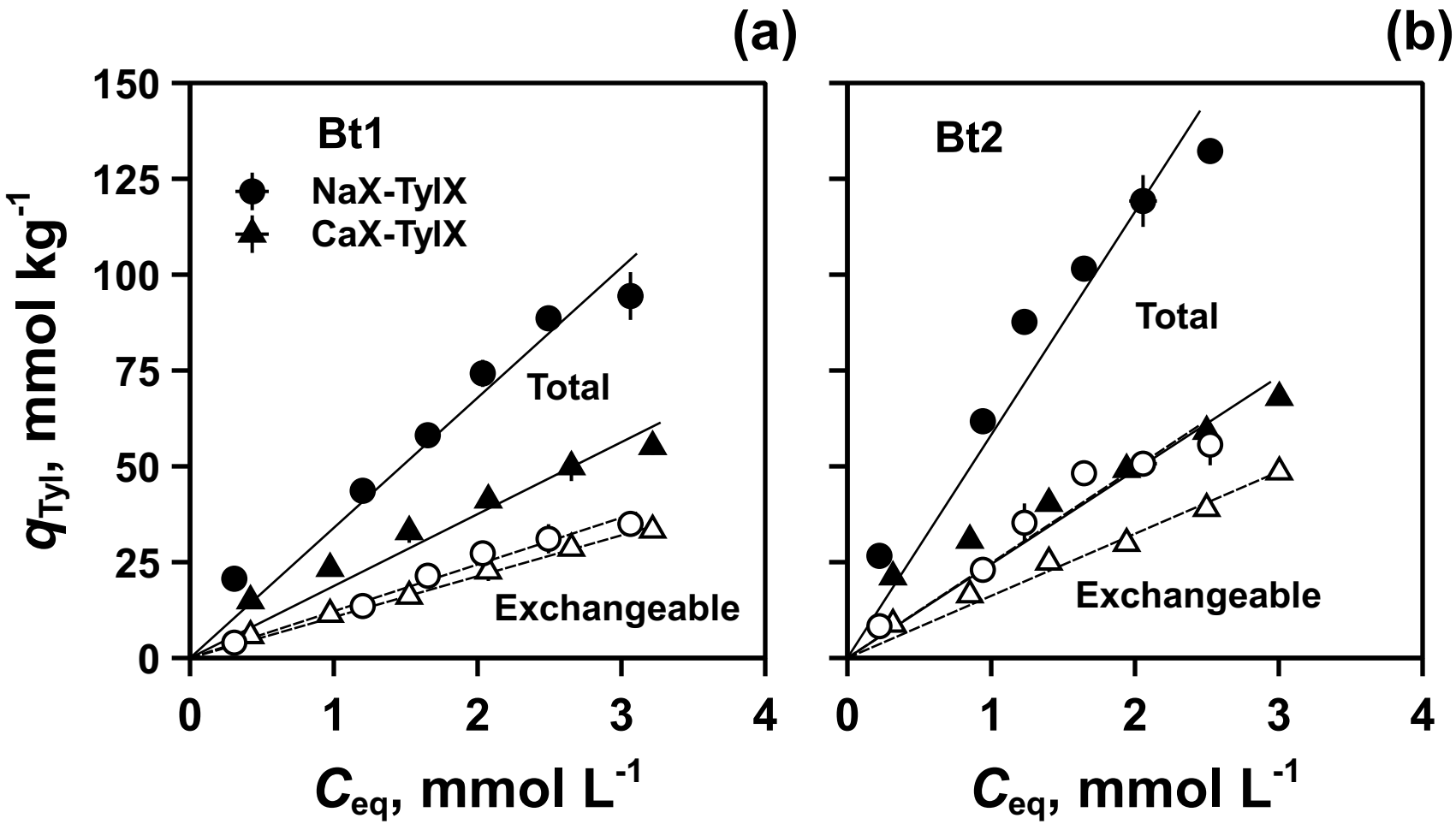
(a)
(b)
Bt1
Bt2
NaX-TylX
CaX-TylX
Total
Exchangeable
Total
Exchangeable
q_{Tyl}, mmol kg^{-1}
C_{eq}, mmol L^{-1}
C_{eq}, mmol L^{-1}
0
25
50
75
100
125
150
0
1
2
3
4
0
1
2
3
4

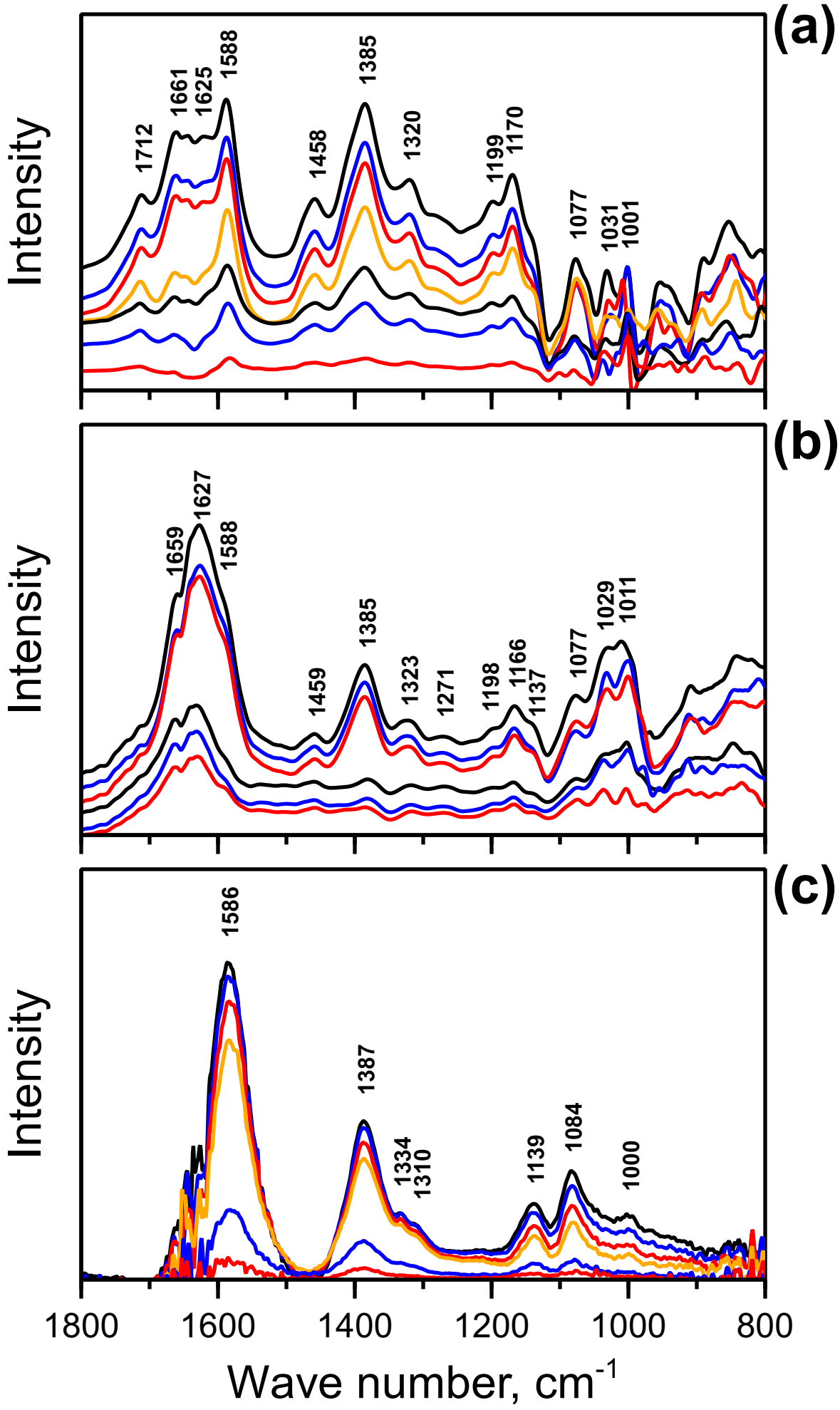
(a)
Intensity
1712
1661
1625
1588
1458
1385
1320
1199
1170
1077
1031
1001
(b)
Intensity
1659
1627
1588
1459
1385
1323
1271
1198
1166
1137
1077
1029
1011
(c)
Intensity
1586
1387
1334
1310
1139
1084
1000
1800
1600
1400
1200
1000
800
Wave number, cm-1

Table 1

Linear partition coefficients (K_P in L kg^{-1}) that describe the tylosin adsorption isotherms in Fig. 5 as a function of competing cation and soil horizon.

	Total			Exchangeable			Nonexchangeable		
Horizon	K_P	SE[a]	CI[b]	K_P	SE	CI	K_P	SE	CI
				NaX-TylX					
Bt1	34.0	0.91	1.9	12.2	0.32	0.7	21.8	0.76	1.6
Bt2	58.2	1.83	3.9	24.8	0.84	1.8	33.4	1.38	2.9
				CaX_2-TylX					
Bt1	18.8	0.63	1.3	10.7	0.19	0.4	8.09	0.52	1.09*
Bt2	24.5	0.98	2.1	16.2	0.33	0.7	8.27	0.76	1.61

[a]Standard error of K_P.

[b]The 95% confidence interval associated with K_P.